Use of Thermodynamic Modeling for Selection of Electrolyte for Electrorefining of Magnesium from Aluminum Alloy Melts

Adam J. Gesing & Subodh K. Das

Metallurgical and Materials Transactions B

ISSN 1073-5615

Metall and Materi Trans B
DOI 10.1007/s11663-016-0724-8

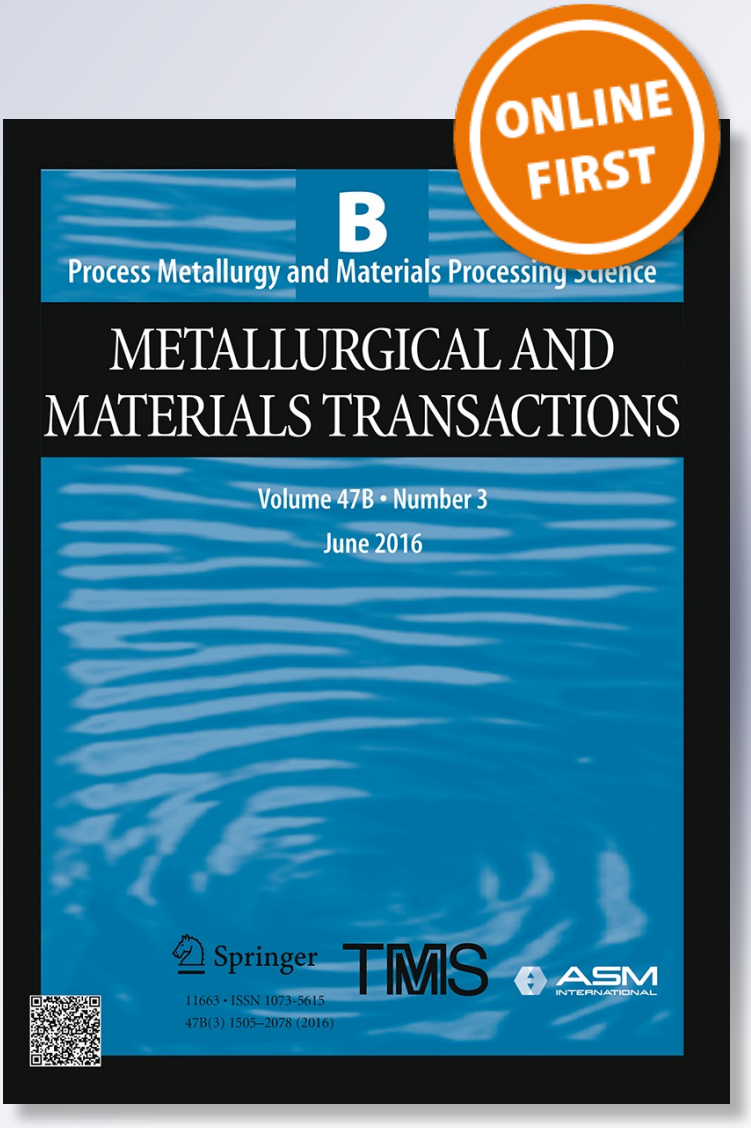

Springer

Use of Thermodynamic Modeling for Selection of Electrolyte for Electrorefining of Magnesium from Aluminum Alloy Melts

ADAM J. GESING and SUBODH K. DAS

With United States Department of Energy Advanced Research Project Agency funding, experimental proof-of-concept was demonstrated for RE-12^{TM} electrorefining process of extraction of desired amount of Mg from recycled scrap secondary Al molten alloys. The key enabling technology for this process was the selection of the suitable electrolyte composition and operating temperature. The selection was made using the FactSage thermodynamic modeling software and the light metal, molten salt, and oxide thermodynamic databases. Modeling allowed prediction of the chemical equilibria, impurity contents in both anode and cathode products, and in the electrolyte. FactSage also provided data on the physical properties of the electrolyte and the molten metal phases including electrical conductivity and density of the molten phases. Further modeling permitted selection of electrode and cell construction materials chemically compatible with the combination of molten metals and the electrolyte.

DOI: 10.1007/s11663-016-0724-8

I. INTRODUCTION

A recently published paper[1] describes the process details, experimental results and product marketability, and economic analysis of the process for extracting a desired amount of magnesium from secondary aluminum scrap melts using an electrorefining technology. The project was funded by the United States Department of Energy Advanced Research Project Agency.[4]

North America produces only ~70,000 tonnes of primary Mg annually. The only practical recycling of postconsumer Mg is as alloying content in the Al alloy recycling system. However, in that system, over 30,000 tonnes of Mg content is chlorinated or fluxed out of Al to end up as Mg chloride contamination of dross.[1] An economical, environmentally friendly, and chlorine-free Mg recovery process could be disruptive and transformational for the Mg production industry by enabling the recycling of 30,000 tonnes of primary quality Mg annually.

An experimental proof-of-concept was demonstrated for a patent-pending[2] and trademark-pending[3] RE12^{TM} process for extracting a desired amount of Mg from recycled scrap secondary Al melts. Mg was extracted by electrorefining producing Mg product suitable as Mg alloying hardener additive to primary grade Al alloys. This efficient electrorefining process operates at high current efficiency, high Mg recovery, and low-energy consumption. Mg electrorefining product can meet all the impurity specifications with subsequent melt treatment for removing alkali contaminants. All technical results obtained in the RE12^{TM} project indicate that the electrorefining process for extraction of Mg from Al melt is technically feasible. A techno-economic analysis indicates high potential profitability for applications in Al foundry alloys as well as beverage can and automotive sheet alloys. The combination of technical feasibility and potential market profitability completes a successful proof-of-concept.

The compositions of the electrolytes for the electrorefining cell were explored. The preferred composition was selected using the best available information and tools. These included the molten salt literature and the commercially available FactSage software program for thermodynamic and phase diagram calculations.[6–25] FactSage[5] includes the thermodynamic and material property databases, and computational models. FactSage is a fully integrated thermochemical database that couples proven FactSage software with self-consistent critically assessed FACT thermodynamic data.

The research team prepared and characterized the electrolyte composition required for the electrorefiner, and demonstrated that the electrolyte composition can be maintained and cleaned of oxide contamination.

II. PROCESS CONCEPT

The process concept for extraction of Mg from Al scrap was designed to fit with existing Al remelting and recycling processes. Al is typically resmelted in a sidewall reverberatory furnace and the Mg is chlorinated out of the melt by continuous injection of Cl_2 gas through the circulation pump impeller throughout the

ADAM J. GESING, formerly Technical Director with Phinix, LLC, Lexington, KY, is now President, Gesing Consultants Inc., Toronto, Canada. SUBODH K. DAS, CEO, is with Phinix, LLC. Contact e-mail: skdas@phinix.net
Manuscript submitted December 30, 2015.

Published online: 23 June 2016

melting cycle. In this conventional system, continuous chlorination ensures that the Mg concentration in the metal heel in the furnace is always maintained at the product specification concentration. In the RE12™ process, Cl_2 injection and Mg chlorination are replaced by Mg electrorefining and Mg recovery for recycling. The melt from the melting furnace sidewall is continuously recirculated through the electrorefining cell again, always maintaining the Mg concentration at the product specification level. The excess Mg present in the scrap feed is extracted and collected as Mg with very minor Al content. Magnesium is removed from the electrorefiner as a continuously cast solid rod, thus avoiding problems of handling and protecting from oxidation of molten Mg. The Al product is on specification and follows existing melt treatment and casting procedures. The Mg solid rod product is ready for sale as an Mg addition for Al-Mg alloys. Al alloy melts, batched from prime Al, are always treated for removal of alkali and alkaline earth contaminants (Na and Ca). This standard treatment will also deal with any residual LiF or Li content of the Mg hardener product. Figure 1 schematically illustrates the RE12™ process concept and its conceptual integration with an Al melter in an Al secondary smelter.

III. ELECTROLYTE SELECTION

Electrolyte composition was selected based on both thermodynamic calculations using the FactSage thermodynamic databases and free energy minimization software that calculates phase diagrams and chemical equilibria. Electrolytes were selected for laboratory experiments that best meet the following criteria:

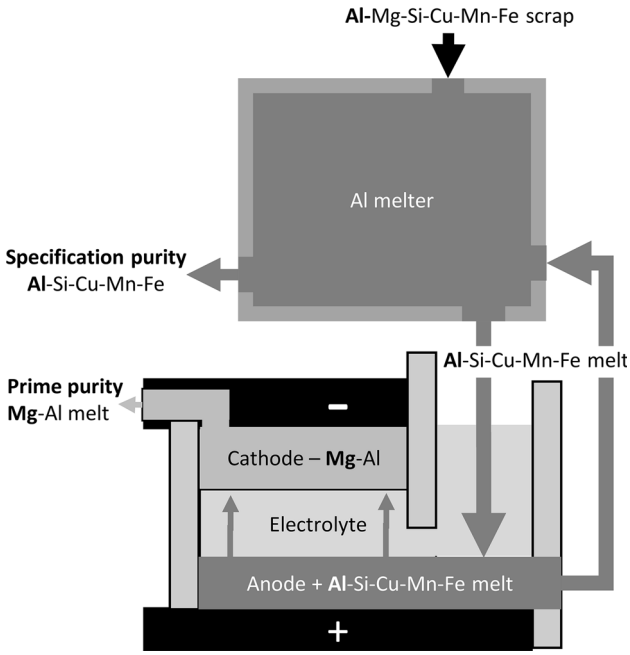

Fig. 1—Concept of Mg electrorefining cell linked to Al scrap melter.

- Melt density at 1073 K (800 °C): ~2.05 g/cm^3

  To separate the Al feed melt from Mg product melt by density, the electrolyte should have a density half way between that of the Al and Mg melt at the operating temperature of ~1073 K (800 °C): Al-2.3 g/cm^3, Mg-1.6 g/cm^3 gives ~2 g/cm^3 for electrolyte. For fluorides, only binary LiF-MgF_2 mixtures could achieve the target melt density, while maintaining sufficient Mg^{2+} concentration for efficient Mg^{2+} supply at the cathode.
- Ability to transport both Mg^{2+} and Al^{3+} ions and electrodeposit them as metal on the cathode

  Fluoride salt mixtures of alkali and alkaline earth elements are able to transport both Mg^{++} and Al^{+++} ions and electrodeposit them in Mg metal on the cathode. Mg alloying element has the most negative electrode potential in the anode metal pool so it is the first metal to be oxidized at the anode and transferred to the electrolyte. Any Li contamination of the Al-Mg anode melt pool resulting from the $3LiF + Al \rightarrow 3Li + AlF_3$ or $2LiF + Mg \rightarrow 2Li + MgF_2$ salt-metal equilibria is oxidized at the anode before Mg extraction. The anode Al has the next highest electrode potential, hence once Mg is depleted from the anode surface and Al is next to be oxidized and transferred to the electrolyte. Conversely at the cathode, Mg^{2+} must have the highest electrode potential of the ion components of the electrolyte in order for the Mg to be deposited first at the cathode. Al^{3+} has a higher electrode potential and any Al oxidized at the anode is transported to the cathode and deposits in the cathode pool in preference to Mg.
- Maximum ionic conductivity

  Li^+ is the smallest metallic cation with the highest mobility, and Li metal atom has the lowest solubility in both chloride and fluoride salts. This provides the selected LiF-MgF_2 fluoride electrolyte composition with the highest ionic conductivity and the lowest electronic transport number, leading to a predicted current efficiency of >99 pct.
- Transport numbers: Ionic ~100 pct; electronic: ~0 pct

  The very high current efficiency demonstrated in the electrorefining experiments indicates that ions (mainly Li^+) carry virtually all the electrical current through the electrolyte and that the contribution of electron conduction is negligible for the LiF-MgF_2 electrolyte system.
- Minimum susceptibility to hydrolysis

  Thermodynamic equilibrium calculations indicate that the selected LiF-MgF_2 fluoride electrolyte composition is stable in contact with moist air at the cell operating temperature. This will allow operation of nonhermetically sealed industrial cells. Electrolyte, dried and batched and premelted as described above in the experimental section, still reacted visibly with the Al-Mg anode alloy melt evolving H_2 gas bubbles and precipitating solid oxides particles. The mass balance on the metal and the electrolyte quantity and composition indicated that even after melting the electrolyte still contained ~5 wt pct H_2O, presumably still complexed with MgF_2 or as OH^- ion. That water, or OH^-, had to be eliminated before Mg elec-

trorefining could commence. A preliminary experiment indicated that cleanup by pre-electrolysis of $H_2O + ½ C \rightarrow H_{2(-)} + ½ CO_{2(+)}$ may be an efficient way of per-cleaning the water from the electrolyte. However, for most of the experimental electrorefining runs, the REDOX reaction with the molten metal was employed for drying the melt. Resultant solid oxide particle contamination of the electrolyte observed during the cell post-mortem did not significantly interfere with the electrorefining process. The best results were obtained by refreezing the electrolyte after REDOX cleaning, and separating clean white electrolyte from the oxide sludge, and using the clean, dry electrolyte.

- Chemical compatibility with materials of construction
  LiF-MgF_2 is compatible with Al_2O_3, MgO, AlN, C, Ti, Fe, and TiB_2. This gave a suite of materials for the construction of the laboratory proof-of-concept electrorefiner. CaO reacts with the electrolyte producing CaF_2, eliminating the Ca-aluminate-bonded refractories as potential materials of construction. At 1073 K (800 °C), LiF-MgF_2 has a superheat of ~ 283K (10 °C), making it compatible with electrolyte containment by its own freeze in a full-scale electrorefiner. The preferred refractory is AlN, but Al_2O_3 is also compatible in contact with the Al anode metal pool and MgO is compatible with both electrolyte and the Mg-rich cathode pool.

IV. THERMODYNAMIC MODELING

Thermodynamic, electrochemical, and energy and mass balance calculations have shown that the proposed concept is technically feasible. These calculations indicate that Li, Na, Ca, Sr, and Mg will be selectively removed from an Al alloy melt, with minimum Al oxidation at the submerged anode pool. Li^+, Na^+, Ca^{++}, and Sr^{++} will accumulate in the electrolyte, while any Al^{3+} and Mg^{2+} will be reduced at the cathode forming the floating refined product melt.

Similar principles are being used commercially today to produce high-purity aluminum in the Hoopes cell using industrial-grade aluminum feed. Further, there is a patent literature describing electrolytic recovery of reactive lithium from aircraft manufacturing Al-Li alloy scrap.[1]

A. *Chemical Equilibria and Impurity Contents*

The question may arise of how the proposed electrochemical process could selectively anodically oxidize Mg at such a low concentration without oxidizing the dominant Al content. Also, could Mg anodically oxidize in preference to the other alloying elements?

Answers to these questions can be calculated by comparing first the standard electrode potential ($E°$) of the various elements in the Al alloys at the anticipated reaction temperature of ~1073 K (800 °C). The team calculated the $E°$ for Al and the main alloying elements using the Nernst equation,

$$E° = -\Delta G_f°/nF,$$

where $\Delta G_f°$ is the free energy of salt formation, n is the number of electrons transferred, and F is the Faraday constant. The salt formation reactions are

$$M' + ½ X_2 \rightarrow M'X,\ n = 1$$

$$M'' + X_2 \rightarrow M''X_2,\ n = 2$$

$$M''' + 3/2\ X_2 \rightarrow M'''X_3,\ n = 3$$

$$M'''' + 2\ X_2 \rightarrow M''''X_4,\ n = 4,$$

where X = Cl, F; M′ = Li, Na, K, Cu; M″ = Mg, Ca, Sr, Cu, Fe, Mn, Zn; M‴ = Al, Fe, Mn; and M⁗ = Si, Mn, Sn.

The standard electrode potentials were calculated from the free energy of formation of fluoride or chloride salts based on the liquid standard states at 1073 K (800 °C). They are listed in Table I. The more negative values for the fluoride compounds indicate that these are more stable than chlorides. Similarly, within each chloride or fluoride group, compounds with more negative $E°$ are more stable. Mg salt couple and those above are suitable as electrolyte components, as these will not be reduced at the cathode at potentials below those of the Mg salt couple. Elements below the Mg salt couple will not be oxidized at the anode as long as the Mg is present in sufficient concentration in the anode.

On the fluoride side, only the LiF-MgF_2 system is light enough to satisfy the electrolyte density requirement of ~2 g/cm^3. Chloride salts are less dense, consequently $SrCl_2$ addition can be used to increase the density of $MgCl_2$—(LiCl or KCl or NaCl) mixtures to the desired density. LiCl is difficult to handle because it is highly hygroscopic and deliquescent, and KCl has the lowest ionic conductivity. This leaves NaCl-$MgCl_2$-$SrCl_2$ as a preferred chloride system.

To determine the window of operation for the selective electrochemical dissolution of Mg from Al alloys, one can solve the Nernst equation relating electrode potential to the standard electrode potential and concentration. Mg is the most reactive component of the anode Al alloy; therefore, it sets the anode electrode potential through the equilibrium between $Mg_{(Al)}$ and $Mg^{2+}_{(elect)}$. The concentration of Al^{3+} in the electrolyte at that potential is then determined by the equilibrium between $Al_{(Al)}$ and $Al^{3+}_{(elect)}$. This leads to

$$E°_{Mg/Mg^{2+}} - RT/2F \ln\left(\left[Mg^{2+}_{(elect)}\right]\Big/\left[Mg_{(Al)}\right]\right) = E_{anode} = E°_{Al/Al^{3+}} - RT/3F \ln\left(\left[Al^{3+}_{(elect)}\right]\Big/\left[Al_{(Al)}\right]\right)$$

The concentration of the Al^{3+} in the electrolyte can be calculated from these Nernst equations using the standard electrode potentials $E°$ listed in Table I.

Table I. Standard Potentials for Metal Chloride/Fluoride Salt Couples at 1073K (800 °C)

Metal/Chloride Salt Couple	Standard Potential, $E°$	Metal/Fluoride Salt Couple	Standard Potential, $E°$
K/KCl	−3.452	Ca/CaF_2	−5.354
$Sr/SrCl_2$	−3.432	Sr/SrF_2	−5.286
Li/LiCl	−3.374	Li/LiF	−5.267
$Ca/CaCl_2$	−3.276	Mg/MgF_2	−4.756
Na/NaCl	−3.238	Na/NaF	−4.736
$Mg/MgCl_2$	−2.332	K/KF	−4.716
$Al/AlCl_3$	−1.841	Al/AlF_3	−4.068
$Mn/MnCl_2$	−1.600	Si/SiF_2	−3.638
$Zn/ZnCl_2$	−1.138	Mn/MnF_2	−3.261
$Si/SiCl_4$	−1.200	Zn/ZnF_2	−2.809
$Fe/FeCl_2$	−0.895	Fe/FeF_2	−2.701
$Cu/CuCl_2$	−0.086	Cu/CuF_2	−1.692

The results are illustrated in Figure 2 for 16 MgF_2 + 84 LiF and for 36 $MgCl_2$ + 32 $LiCl_2$ + 32 $SrCl_2$ electrolytes. The target Mg concentrations in the anode product Al alloy range from 1 wt pct for sheet alloys to 0.1 wt pct for foundry alloys. In that concentration range, anodic oxidation of Al is negligible with Al^{3+} concentration in the electrolyte at the anode interface calculated, respectively, at 1×10^{-6} to 3×10^{-5} mol pct for fluoride electrolyte and a factor of three less for the chloride electrolyte.

Hence the electrorefiner is expected to be very selective in removing Mg under quasi-equilibrium conditions. Even at a very low mole fraction of Mg in the Al alloy feed, it is theoretically feasible to electrochemically separate Mg from Al in either fluoride or chloride electrolyte without oxidizing significant amounts of Al at the anode. Chloride provides more than a little more selectivity. Under commercially practical current densities, the anode surface will be continually depleted of Mg and slightly higher rates of anodic oxidation of Al are expected.

Similar Nernst equations can be written for the cathode equilibria that govern element concentrations in the Mg product. For fluoride electrolyte,

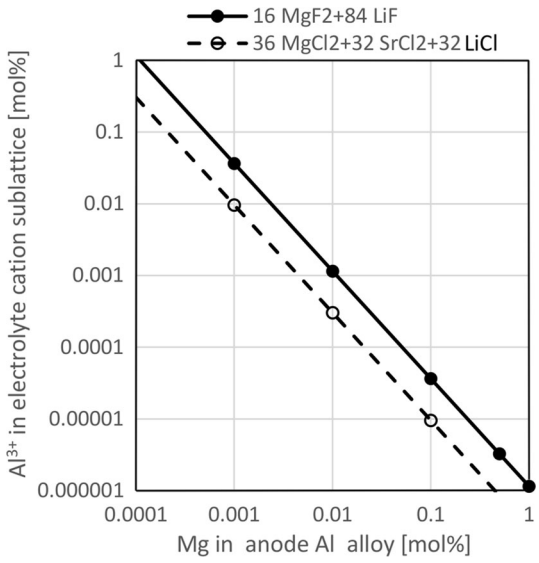

Fig. 2—Selectivity of oxidation at the anode surface—concentration of Al^{+++} in fluoride and chloride electrolytes as a function of Mg concentration in the anode Al alloy at 1073 K (800 °C).

$$-E^{\circ}_{Mg/MgF_2} - RT/2F \ln\left(\left[Mg_{(Mg)}\right] \Big/ \left[Mg^{2+}_{(elect)}\right]\right) = E_{cathode} = -E^{\circ}_{Li/LiF} - RT/F \ln\left(\left[Li_{(Mg)}\right] \Big/ \left[Li^{+}_{(elect)}\right]\right)$$

and for chloride electrolytes:

$$-E^{\circ}_{Mg/MgCl_2} - RT/2F \ln\left(\left[Mg_{(Mg)}\right] \Big/ \left[Mg^{2+}_{(elect)}\right]\right) = E_{cathode} = -E^{\circ}_{Li/LiCl} - RT/F \ln\left(\left[Li_{(Mg)}\right] \Big/ \left[Li^{+}_{(elect)}\right]\right)$$

$$E_{cathode} = -E^{\circ}_{Na/NaCl} - RT/F \ln\left(\left[Na_{(Mg)}\right] \Big/ \left[Na^{+}_{(elect)}\right]\right)$$

$$E_{cathode} = -E^{\circ}_{Sr/SrCl_2} - RT/2F \ln\left(\left[Sr_{(Mg)}\right] \Big/ \left[Sr^{++}_{(elect)}\right]\right)$$

Additional constraints of component concentrations in each phase summing to 1 are also applied. These equations are solved for concentrations of Li or Na and Sr in the Mg product. The results of these calculations are shown in Figures 3 and 4. The electrolyte density constraints limit the $MgCl_2$ concentration between 28 and 44 mol pct or 16 and 36 mol pct in, respectively, the chloride electrolytes based on Li^+ and Na^+. Within these ranges, the Li contamination of Mg product is predicted to be between 0.01 and 0.02 mol pct, while Na would be between 0.08 and 0.16 mol pct and Sr would range between 0.8 and 2.7 mol pct. In the fluoride electrolyte, the density constrains the MgF_2 concentration between 13 and 19 mol pct leading to Li concentration in the electrolyte of ~0.8 mol pct.

The Li concentration In Mg drops drastically to ~0.004 mol pct as the MgF_2 concentration approaches 100 mol pct. This suggests that Li could be extracted from the cathode product by equilibrating it with a salt flux with a high Mg^{2+} concentration. Commercially, carnallite $KCl{\cdot}MgCl_2$ is sometimes used as molten flux for extraction of alkali contaminants from either Al- or Mg-based melts.

B. *Phase Diagrams*

The FactSage phase diagram module was used to identify the extent of the one-phase molten salt field for

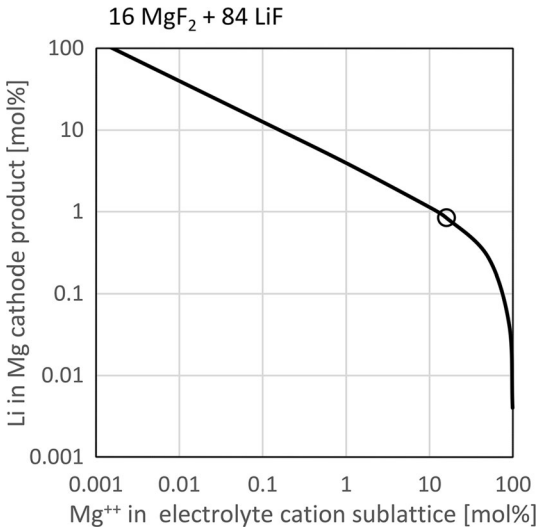

Fig. 3—Calculated equilibrium concentration of Li in Mg product with 84 LiF + 16 MgF_2 electrolyte at 1073 K (800 °C).

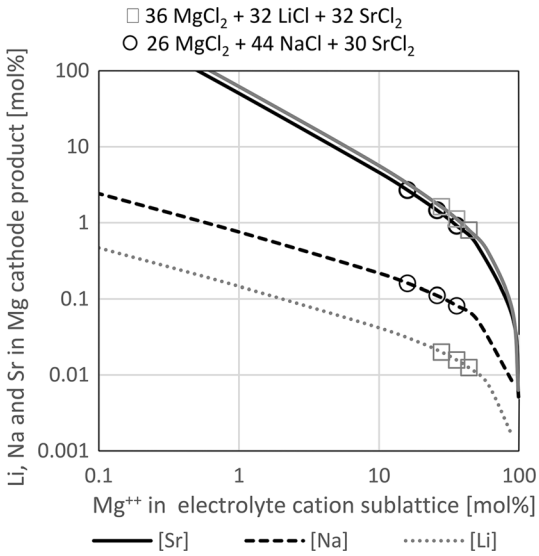

Fig. 4—Calculated equilibrium concentration of Li or Na and Sr of Mg cathode product in chloride electrolytes. The electrolyte density constraints limit the Mg^{++} concentration between 28 and 44 mol pct for Li^+-based electrolyte and 16 and 36 mol pct for Na^+-based electrolytes at 1073 K (800 °C).

the (LiF)-(MgF_2) binary fluoride system as well as the LiCl/NaCl/KCl—$MgCl_2$—($SrCl_2$)/($CaCl_2$) ternary chloride systems (Figures 5 and 6). This information was combined with the salt melt properties also supplied by the FactSage salt system database. In the fluoride system, only a binary combination of LiF and MgF_2 could satisfy the density constraint of ~2 g/cm^3. Combinations containing NaF, KF, CaF_2, or SrF_2 were too dense. Chlorides are less dense and a substantial addition of $SrCl_2$ is needed to bring the density up to ~2 g/cm^3. LiCl is hygroscopic to the point of deliquescence; $MgCl_2$ hydrolyzes as $MgCl_2 \cdot (H_2O)_x$, $x = 1, \ldots, 6$ and cannot be dehydrated by heating alone without conversion into MgO + HCl; KCl has the lowest ionic conductivity and the highest solubility for K metal; NaCl is the lowest cost. Consequently, NaCl-$SrCl_2$-$MgCl_2$ and LiF-MgF_2 systems were selected for further consideration.

C. *Physical Properties*

1. *Density*

The specific compositions of the prospective fluoride and chloride systems were selected based on the melt densities calculated by FactSage from the Salt database (Figures 7 and 8). The density target of 2.05 g/cm^3 was selected to be half way between the densities of the Al anode and Mg cathode melts at 1.7 and 2.4 g/cm^3. The calculated density values at 750 °C for the (26 $MgCl_2$ + 44 NaCl + 30 $SrCl_2$) melt are approximate since the NaCl-$SrCl_2$ and $MgCl_2$-$SrCl_2$ binary liquids are assumed to be ideal in terms of the volumetric properties (i.e., the excess volumes for these two binary subsystems were not modeled). Addition of MgF_2 to LiF increases the density, while $MgCl_2$ addition decreases the density of the 60 NaCl + 40 $SrCl_2$ mixture. The slope of the lines on the fluoride plot is steeper translating to a narrower allowable composition window for the fluoride electrolyte than for the chloride.

2. *Electrical conductivity*

In practical terms, the ionic conductivity of the salt melt is set by the mobility and the concentration of the fastest monovalent cation in the melt. Smaller ions move faster, hence it is expected that ionic conductivity of $Li^+ > Na^+ > K^+$. This is borne out in the ionic conductivity estimates produced based on the FactSage equilibrium calculations which give the molar concentrations of each of the ionic and metallic species in the molten electrolyte composition.

A theoretical model based on the Modified Quasi-chemical Model[26–28] has been developed for the electrical (ionic) conductivity of multicomponent inorganic molten salts and was applied successfully to the NaCl-KCl-$MgCl_2$-$CaCl_2$ and NaF-AlF_3-CaF_2-Al_2O_3-LiF-MgF_2 electrolytes (the latter is used to produce aluminum by the Hall–Héroult process) by the FactSage research group. This model has not been published yet; in particular, it uses the number of moles of the various quadruplets calculated from the previously developed thermodynamic model (where each quadruplet is formed of two cations and two anions) and the molar volume calculated from the previously developed density model.[29,30] The model parameters are the mobilities of the ions associated with the various quadruplets. The ionic conductivity model for the NaF-AlF_3-CaF_2-Al_2O_3-LiF-MgF_2 electrolyte will soon be implemented in the FThall public database of FactSage.

The electronic conductivity was estimated according to the procedure proposed by Wilson.[31] The assumptions of Wilson are as follows: (i) The valence electrons of the dissolved metal become the conduction electrons of the system; (ii) The electrons are in plane-wave states and are scattered by the pseudo-potentials; (iii) The scattering of the electrons can be described by first-order time-dependent perturbation theory. Thereafter, the resistivity ρ (and thus the electronic conductivity) of

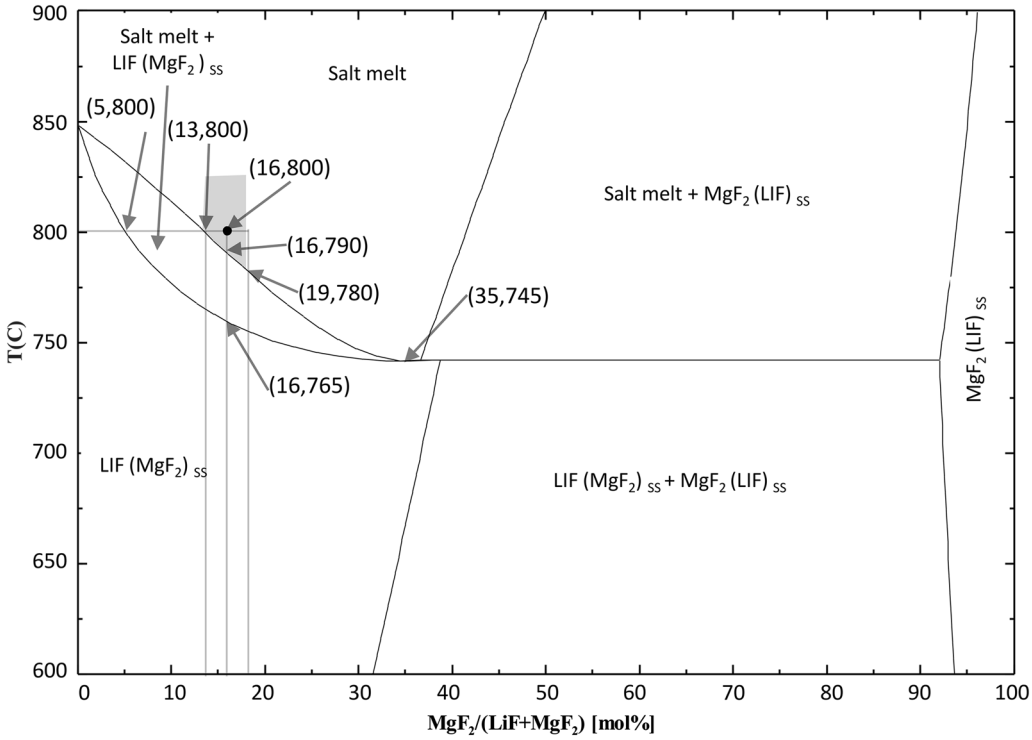

Fig. 5—Calculated LiF-MgF_2 phase diagram showing the selected operating region (in the shaded area) for Mg electrorefining.

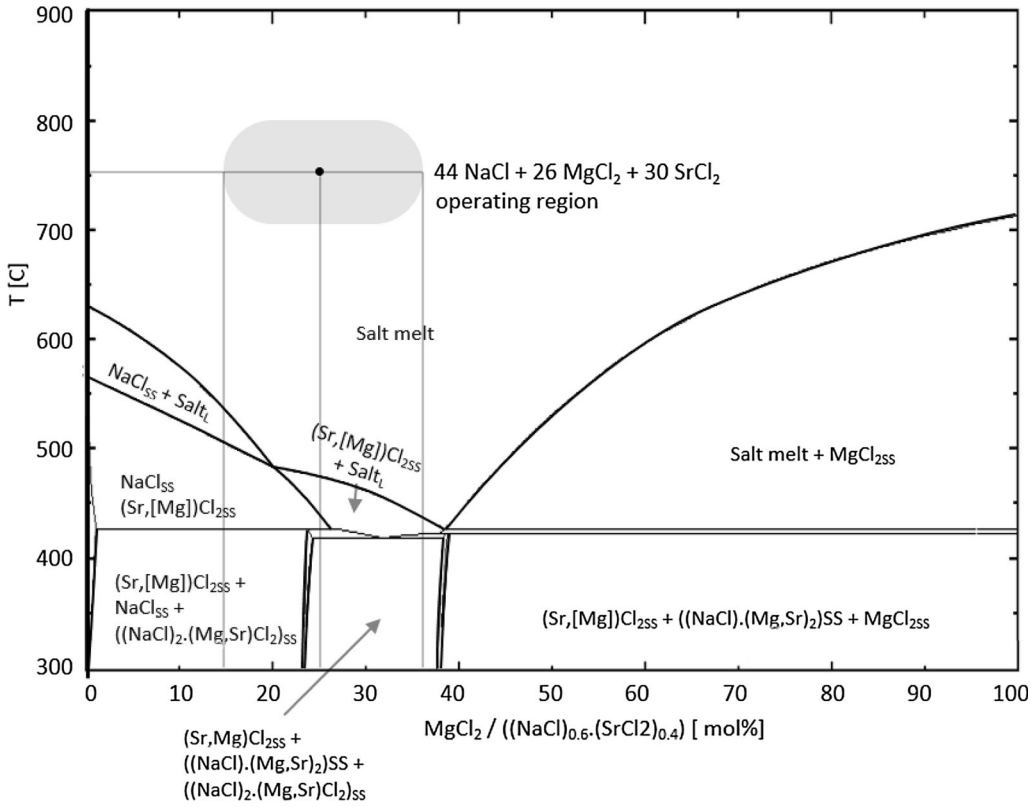

Fig. 6—FactSage-calculated pseudo-binary section through the $MgCl_2$-NaCl-$SrCl_2$ ternary phase diagram at molar (NaCl)/($SrCl_2$) = 60/40. The potential operating region for the 44 NaCl + 30 $SrCl_2$ + 26 $MgCl_2$. Mg electrorefining operating region is shown in the shaded area.

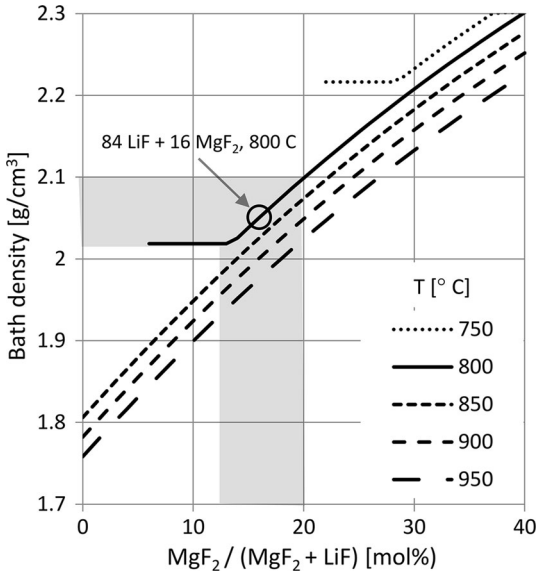

Fig. 7—Selection of the 84 LiF + 16 MgF_2 fluoride electrolyte composition based on salt melt density. At 1073 K (800 °C) lower MgF_2 limit is set by the liquidus at 13 mol pct, and upper limit of 2.1 g/cm^3 is reached at 20 pct.

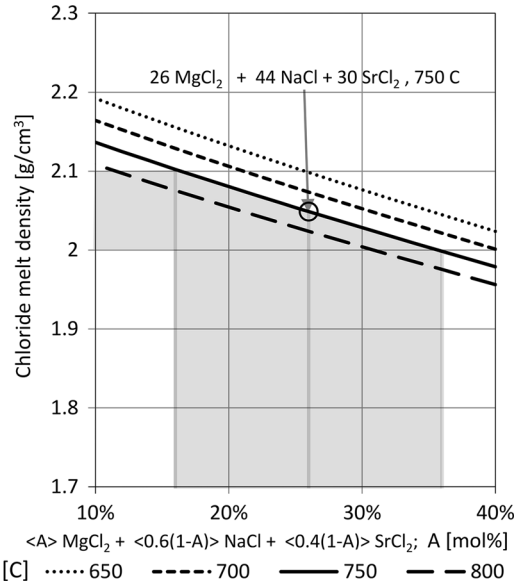

Fig. 8—Selection of the 26 $MgCl_2$ + 44 NaCl + 30 $SrCl_2$ chloride electrolyte composition based on the density target of 2.05 ± 0.05 g/cm^3 at 1023 K (750 °C). This gives an allowable $MgCl_2$ composition range of 16 to 36 mol pct.

an *MX-M* liquid in the region of small metal concentrations can be obtained by solving the Boltzmann equation assuming elastic scattering:

$$\rho = \frac{4(mec)^2}{3\pi\hbar^3 n_e^2}\int_0^{2k_F}\frac{(N_X + N_M)k^3}{\left(k^2+\lambda^2\right)^2}dk,$$

where $\hbar$ and c are, respectively, the reduced Planck constant and the speed of light; m and e are, respectively, the mass and charge of an electron; n_e, N_M, and N_X are, respectively, the electron, metal ion, and halide ion number densities; λ is the electron wave length; and k_F is the Fermi wave vector. All details for the integration of this equation are given in reference.[31] It has to be pointed out that the methodology of Wilson has shown a good predictive capability for several metal/metal halide systems.[31–33] In the present work, the electronic conductivity $1/\rho_{mixture}$ of the (84 mol pct LiF + 16 mol pct MgF_2) melt was assessed at 1073K (800 °C) as a function of the concentration of the dissolved metal, using the following equation:

$$\frac{1}{\rho_{mixture}} = \frac{(1-x_{MgF_2})}{\rho_{LiF}} + \frac{x_{MgF_2}}{\rho_{MgF_2}} = \frac{0.84}{\rho_{LiF}} + \frac{0.16}{\rho_{MgF_2}}$$

At 1073K (800 °C), the 84 LiF + 16 MgF_2 has a predicted ionic conductivity of 7.2 S/cm, while 44 NaCl + 26 $MgCl_2$ + 30 $SrCl_2$ is predicted to be lower than 2.05 S/cm, and 40 KCl + 25 $MgCl_2$ + 35 $CaCl_2$ is at 1.4 S/cm. This is 3 times and 5 times, respectively, lower than LiF-based salt. Voltage drop in the electrolyte is inversely proportional to the electrical conductivity, and hence will be significantly lower in the fluoride system.

Conduction of electricity by electrons does not contribute to electrorefining, thus it constitutes one mechanism of current efficiency loss. There are no free electrons in a molten salt; they are present as neutral metal atoms (Li, Mg, Al) in the case of fluoride electrolyte. The FactSage FThall database has the thermodynamic data for these metals in the fluoride salt solution. To predict the concentrations of minor constituents of the 84 LiF + 16 MgF_2 electrolyte in equilibrium with Al alloy at the anode or with Mg product at the cathode, FactSage equilibrium calculations with the following starting components were considered:

$$\langle A\rangle 100\ Al\ +\ \langle 1-A\rangle (84\ LiF\ +\ 16\ MgF_2),$$
$$\text{where } \langle A\rangle = 0.1, 0.5, 0.9$$

or

$$\langle A\rangle 100\ Mg\ +\ \langle 1-A\rangle (84\ LiF\ +\ 16\ MgF_2),$$
$$\text{where } \langle A\rangle = 0.1, 0.5, 0.9$$

The equilibria were calculated using compound and solution data from the FThall FactSage public database. The FThall database is devoted to the NaF-AlF_3-CaF_2-Al_2O_3-LiF-MgF_2 electrolyte used to produce aluminum. LiF and MgF_2 are only additives, present in small amounts. Therefore, one has to be cautious regarding the calculations for the LiF-MgF_2 binary subsystem. Therefore, the results displayed in Figures 9 and 10 are only approximate. Results are plotted in Figures 9 and 10. Al^{3+} is present as either 4 or 5—coordinated AlF_3 at concentration <0.63 mol pct when there is excess of Al (A = 0.9). This confirms the Nernst equation prediction that the reaction of the Al with the electrolyte is negligible even in the absence of Mg in Al.

The electronic conductivity estimate in Figures 11 and 12 is based on the equilibrium total neutral metal content of the 84 LiF + 16 MgF_2 salt mixture. The

electronic transport number is the ratio of the electronic component of the electrical conductivity to the total conductivity. At 1073 K (800 °C), the electronic transport number is 0.37 pct. This suggests that if other mechanisms of current efficiency loss are successfully controlled, a >99 pct current efficiency could be achieved for the 84 LiF + 16 MgF_2 electrolyte.

A good current efficiency prediction could not be made for the chloride melts, since the corresponding quantitative metal solubility data were not available. However, some metal-salt phase diagrams available in the literature indicate that the solubility of Na or K in their respective chlorides is significantly higher than that of Li. This suggests that the upper limit on the achievable current efficiency would be lower for the NaCl- and KCl-based chloride electrolytes.

The specific energy consumption is directly proportional to the total cell voltage. The target-specific energy consumption for the Mg extraction is <10 kWh/kg Mg. This corresponds to a cell voltage of <4 V. For a refining cell, the overall reaction is

$$\mathrm{Mg}_{(\mathrm{Al})} \rightarrow \mathrm{Mg}_{(\mathrm{Mg})} \text{with } \Delta E^{\circ} = 0, \text{ and}$$

$$E_{\mathrm{conc}} = -\mathrm{RT}/2\mathrm{F}\ \ln\left(\left[\mathrm{Mg}_{(\mathrm{Mg})}\right] \Big/ \left[\mathrm{Mg}_{(\mathrm{Al})}\right]\right) \approx \mathrm{RT}/2\mathrm{F}\ \ln\left(\left[\mathrm{Mg}_{(\mathrm{Al})}\right]\right) \text{ at } \left[\mathrm{Mg}_{(\mathrm{Mg})}\right] \approx 1$$

E_{conc} is a potential due to Mg concentration difference in the anode and cathode melts. There are two levels of Mg in Al product that are of commercial interest: ~0.1 pct for Al foundry alloys, and ~1 pct for Al sheet alloys. At these levels, E_{conc} evaluates respectively to −0.3 V and to −0.2 V. Since there are other overpotentials and resistances in the cell, the sum of the electrolyte voltage drop and the concentration potential is less than the minimum required for the electrorefining process. Consequently, in order to meet the project target-specific energy consumption target, it is necessary to target an electrolyte voltage drop of <3 V. For the chloride electrolyte, this can be achieved at a realistic commercial current density of 1.5 A/cm^2 only at an unrealistically low anode–cathode distance, ACD, of 4 cm for commercially sized cells. At a realistic ACD of 8 cm, the chloride cell is limited to a current density, CD, of <0.7 A/cm^2. This increases the capital cost of the cell, which scales inversely with the CD.

For fluoride electrolyte with 3 times higher electrical conductivity, the picture is much brighter. The target electrolyte voltage drop of <3 V can be achieved at a realistic 8 cm ACD with a high CD of 2.8 A/cm^2, which

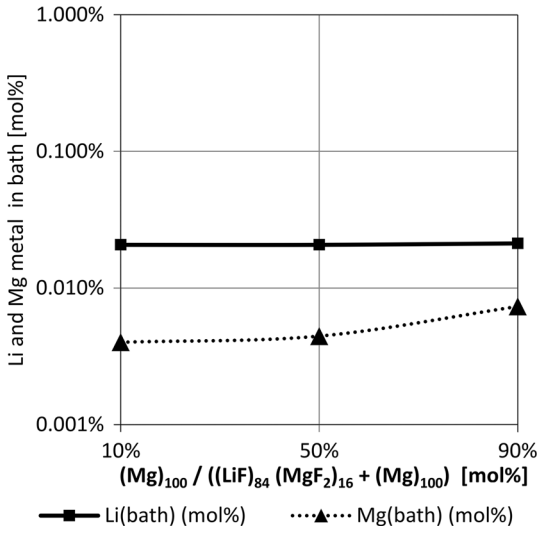

Fig. 10—FactSage equilibrium calculation results for metallic Li and Mg concentrations in 84LiF + 16 MgF_2 salt bath in equilibrium with Mg at 1073 K (800 °C).

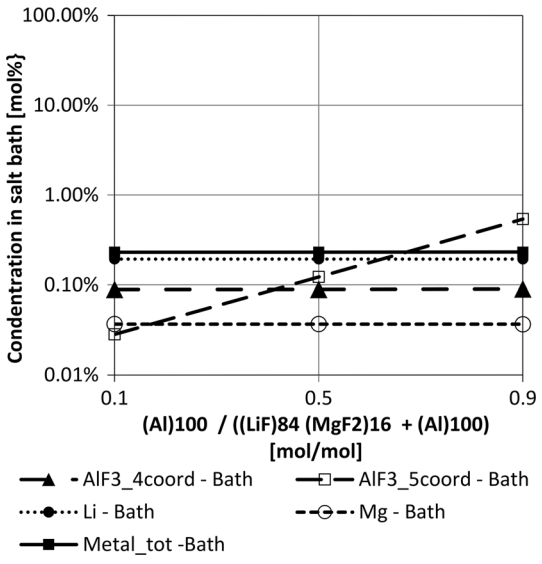

Fig. 9—FactSage-calculated 84 LiF + 16 MgF_2 bath minor component concentrations in equilibrium with Al at 1073 K (800 °C).

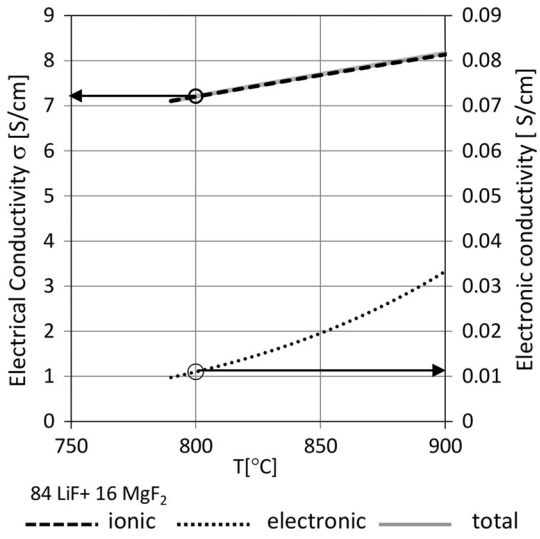

Fig. 11—Ionic and electronic components of the electrical conductivity estimates of the 84 LiF + 16 MgF_2 salt bath at 1073 K (800 °C). The electronic transport number at 800 °C is 0.37 pct. That is equal to current efficiency loss due to electronic conduction through the bath.

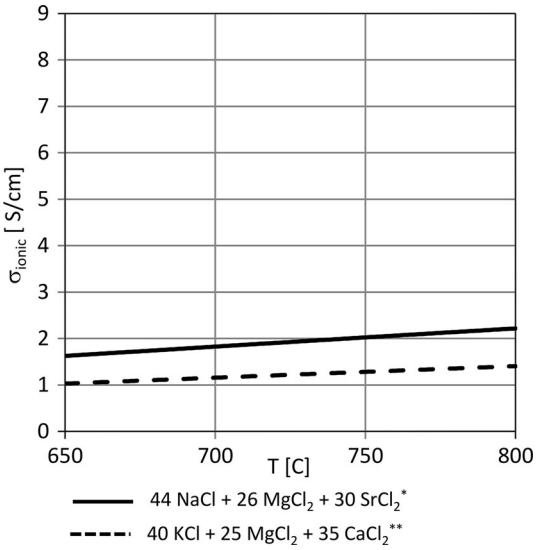

Fig. 12—Ionic conductivity estimates for the potential chloride electrolyte compositions. The values of 1.4 and 2.2 S/cm at 1073 K (800 °C) are ~5 times and ~3 times lower than those for the LiF-based electrolyte. *A. Gesing; **C. Robelin.

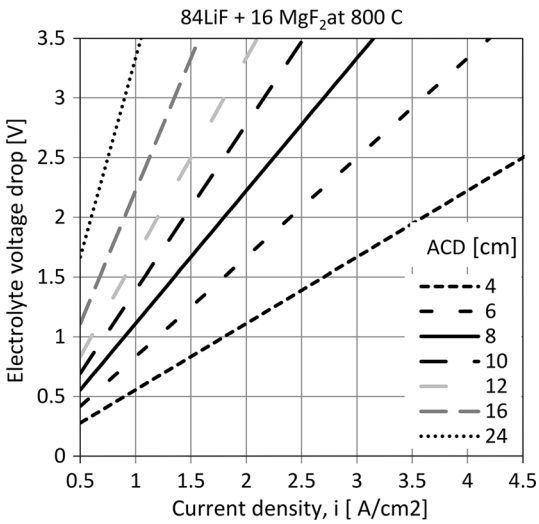

Fig. 13—Resistive voltage drop through 84 LiF + 16 MgF_2 electrolyte as a function of current density at ACD ranging from 4 to 24 cm and at 1073 K (800 °C).

promises significant capital cost savings in comparison with an electrolyte using chloride electrolyte.

Figures 13 and 14 show cell voltage calculations for fluoride and chloride systems, respectively.

3. *Viscosity*

Knowledge of the electrolyte viscosity is important in the design of the internal cell flows and in the filtration of the electrolyte to separate and collect the Mg product droplets from it. FactSage provides calculated viscosity of the NaF-AlF_3-CaF_2-Al2O_3-LiF-MgF_2 electrolyte as a function of temperature and composition. The viscosity of the LiF-MgF_2 liquid was NOT modeled in FactSage. (On the other hand, the viscosity of the NaF-MgF_2 liquid was

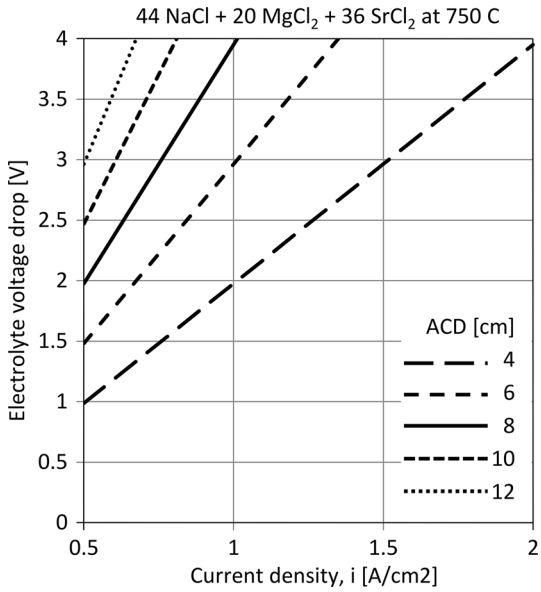

Fig. 14—Resistive voltage drop in the electrolyte as a function of uniform current density for 44 NaCl + 36 $SrCl_2$ + 20 $MgCl_2$ electrolyte at 1023 K (750 °C).

modeled, since NaF is present in large amounts in conventional electrolytes.) Therefore, the values displayed in Figure 15 provide only best available estimates of LiF-MgF_2 salt bath viscosity.

4. *Cell construction materials*

Fact sage reaction, equilibrium and phase diagram modules were used to evaluate the compatibility of the potential cell construction materials with the cell liquids and with the cell atmosphere. Oxide ion, $O^{=}$, solubility in the electrolyte in equilibrium with Al or Mg is limited by the formation of solid oxide precipitates of MgO, MgO·Al_2O_3 or Al_2O_3 depending on the respective activities of Mg and Al. Figure 16 illustrates a FactSage-calculated pseudo-binary section through the LiF-MgF_2-MgO phase diagram.

The edge of the $bath_{(L)}$ field in contact with the $MgO_{(s)}$ field gives the MgO solubility, which at a 1073 K (800 °C) electrorefining operating temperature is only 0.04 wt pct, and the solubility of Al_2O_3 or MgO·Al_2O_3 is even smaller. These refractory materials then provide a convenient set of electrical insulators for the construction of the electrorefining cell. They need to be pure, as common binding phases contain CaO, SiO_2, or FeO. Si or Fe components are reduced by both Al and Mg, and the reduction is accelerated by the presence of the fluoride electrolyte. CaO reacts directly with MgF_2 or $MgCl_2$ to yield $CaCl_2$ or CaF_2 in the electrolyte and solid MgO. AlN and AlON are also electrically insulating and are predicted by FactSage to be inert in contact with molten electrolyte and the anode or cathode metal melts, but are more expensive and difficult to obtain in sizes required for commercial cell refractories. BN was predicted by FactSage to react at 1073 K (800 °C) with both Al and Mg to yield AlN and AlB_{12} or Mg_3N_2 and MgB_2. Since BN is often used as a structural component

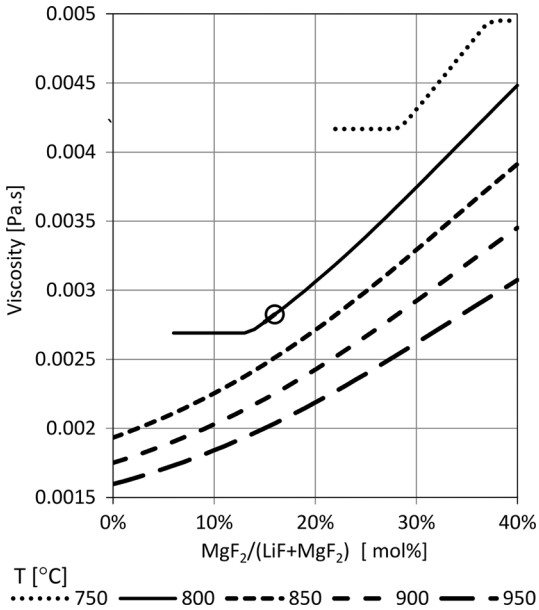

Fig. 15—Viscosity [Pa s] of LiF-MgF_2 salt bath.

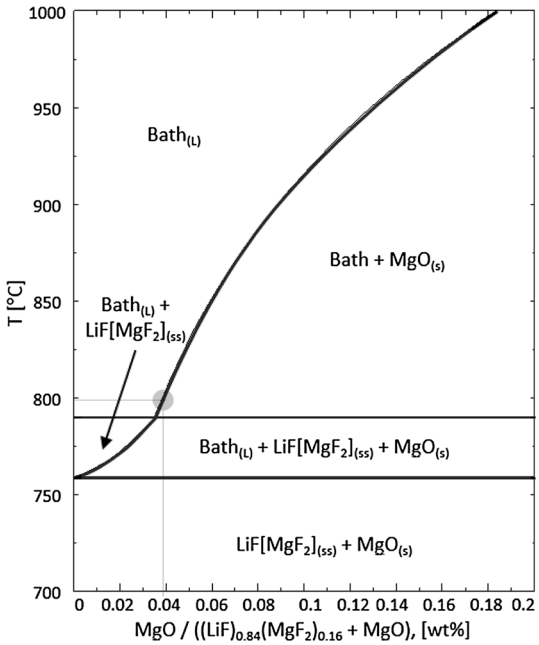

Fig. 16—FactSage-calculated pseudo-binary electrolyte-MgO phase diagram demonstrating MgO solubility in $(MgF_2)_{16}(LiF)_{84}$.

in molten Al, it is likely that the AlN reaction product forms a protective layer on BN.

Iron is an electronic conductor with a very small solubility in molten Mg. It is often used in laboratory cells as a low-cost, Mg-wettable cathode surface and cathode current conductor. However, at 1073 K (800 °C), Fe and most of its alloys creep, and thus cannot be used as long-term structural elements. Graphite is also electronically conducting, is available in large machinable blocks at an affordable cost, and is structurally sound at 1073 K (800 °C). FactSage predicts the formation of Al_4C_3 in contact with Al at 800 °C, and at lower temperatures there is the literature indicating possible formation of intercalation phases with Li or Na. Experimentally, these reactions were not observed and graphite was compatible and structurally stable in contact with both chloride and fluoride electrolyte baths and with anode and cathode metal melts.

5. *Vapor pressure*

FactSage predicts the composition of the gas phase in equilibrium with the liquids and solids in a closed cell. Figures 17 and 18 show the vapor pressures in equilibrium with the 84 LiF + 16 MgF_2 electrolyte and, respectively, with Mg cathode melt and Al anode melt. At 1073 K (800 °C), at the cathode, $Mg_{(g)}$ is the predominant vapor component with a vapor pressure of 0.04 bar, followed by $Li_{(g)}$ at 7E-5 bar and then by $(LiF)_{2(g)}$ at 1.5E-5 bar. In equilibrium between the Al anode melt and the electrolyte, Mg vapor pressure drops to 4E-4 bar, $(LiF)_{2(g)}$ stays at 1.5E-5 bar, and $Li_{(g)}$ and $AlF_{(g)}$ each contribute 7E-6 bar. Mg vapor pressure at the cathode interface is significant, and needs to be contained to prevent Mg evaporation losses. This can be done by designing an Mg collection chamber with no open gas–liquid interface.

6. *Superheat*

Electrolyte evaporation can be controlled by containing it in its own freeze and under its own crust. Such freeze and crust are naturally chemically compatible with the molten electrolyte; they are gas- and liquid-tight and are self-healing. Traditionally, side freeze and frozen crust are used commercially in Al reduction cells to contain NaF-AlF3 fluoride electrolyte and molten Al product. These cells operate at a temperature that gives a 10 °C superheat above the cryolite liquidus surface. It is this low superheat that allows the containment of the cell liquids in the freeze and crust. Figure 19 shows the superheat across the operating composition range for the LiF-MgF_2 electrolyte at the 1073 K (800 °C) operating temperature. Superheat is 10 °C at the target 84 LiF + 16 MgF_2 composition.

Electrorefining cells do not produce gasses. Laboratory cells are typically closed, and are evacuated and are then back filled, and purged with argon. Large commercial electrorefining cells would be less expensive to build and be easier to maintain if they could be operated open to air atmosphere. Containment of cell liquids by freeze and crust enables such a design. Freeze seals the porosity in the refractories making them impermeable to air, thus protecting the graphite and metal components from oxidation. Crust provides a heat radiation barrier and thermal insulation, and seals in the electrolyte vapors. An outer steel shell provides structural support for insulating refractories and while further restricting the air access to the hot interior.

V. EXPERIMENTAL CONFIRMATION

The details of the experimental proof-of-concept of the RE-12^{TM} Mg recovery electrorefining process have

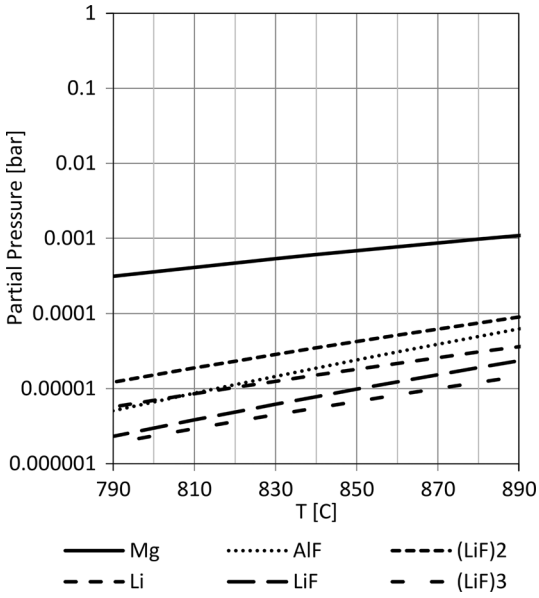

Fig. 17—Vapor species in gas phase in equilibrium with electrolyte and anode metal: 84 LiF + 16 MgF_2 + $Al_{98.5}$ $Mg_{1.5}$.

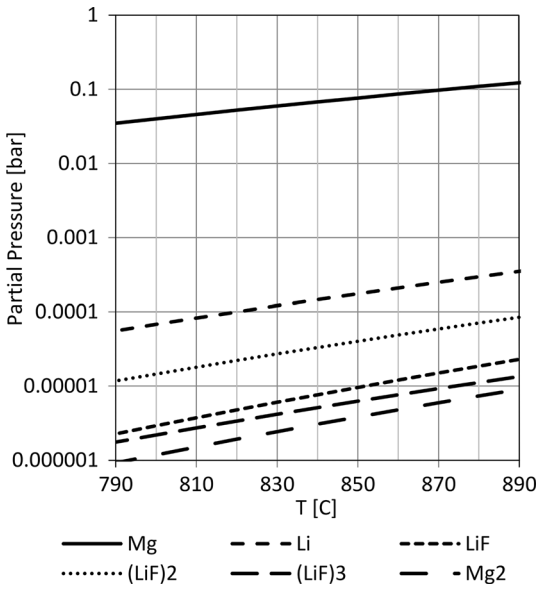

Fig. 18—Vapor species in gas phase in equilibrium with electrolyte and cathode metal: 84 LiF + 16 MgF_2 + $Al_{98.5}$ $Mg_{1.5}$.

already been described in detail.[1] The key results are summarized here, leading to the validation of the FactSage predictions. Table II gives the laboratory-demonstrated parameters of the RE-12^{TM} process.

For LiF-MgF_2 electrolyte, the elemental chemical (ICP) analysis of the products is given in Tables III and IV. For chloride NaCl-$SrCl_2$-MgF_2 electrolyte, as predicted there was significant contamination of the Mg product by Na, 2.5 wt pct and smaller by Sr, 0.35 wt pct.

Figure 20 shows the cell voltage as a function of current density at 1083 K (810 °C), with 84 LiF + 16 MgF_2 electrolyte and ACD of ~7 cm. The measured cell

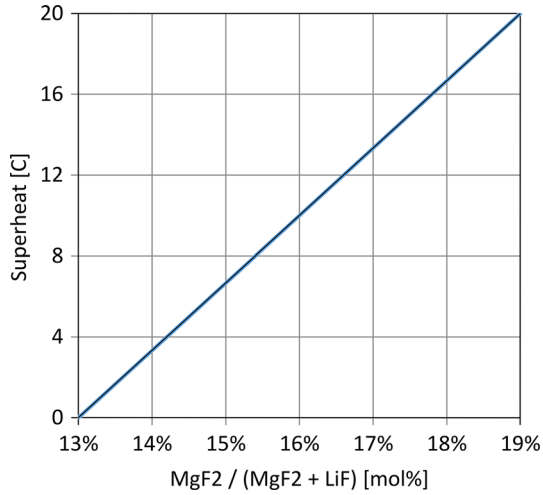

Fig. 19—Superheat, $T_{oper.} - T_{liquidus}$ at $T_{oper.} = 1073$ K (800 °C) as a function of LiF-MgF_2 electrolyte composition across the whole operating range. 10 °C superheat is typical for commercial cells operating with freeze and crust.

voltage values are in the right range based on the predictions coming from FactSage and shown in Figures 13 and 14. Also as predicted, significantly higher cell voltages were recorded with chloride electrolyte at comparable current densities as shown in Figure 21.

VI. COMPOSITIONAL STABILITY

Chemical composition stability of the electrolyte over time is a potential concern. To address this issue, electrolyte over the 6-hour electrorefining time was periodically sampled.

The energy-dispersive X-ray (SEM-EDX) measurements were used to demonstrate the composition stability. Since Li is not detected by EDX, the ratio of Mg/F X-ray intensity ratio as a function of time was followed.

Figure 22 shows that there is no statistically significant change in the MgF_2/LiF ratio in the electrolyte during the electrorefining. The slight increase in the X-ray intensity ratio, I_{Mg}/I_F, measurement is consistent with the observed oxidation of Mg and trapping of small MgO particles by the electrolyte.

Stability of the Mg/F ratio indicates that the Mg deposited at the cathode is replaced one for one by Mg extracted from the anode pool. Li losses are too small to affect the electrolyte composition over the time frame of a laboratory electrorefining run.

VII. DISCUSSION

A. *Fluoride Electrolyte*

There is only one viable composition range for fluorides for a 2.05 density system: 84 ± 3 LiF + 16 ± 3 MgF_2.

Table II. Laboratory-Demonstrated Performance of RE12^{TM} Electrorefining Process Utilizing 84 LiF + 16 MgF_2 Electrolyte at 1073 K (800 °C)

Parameter	Achieved	Target
Cell voltage @ CD 0.9 A/cm^2 (V)	1	<4
Specific energy consumption* @ 0.9 A/cm^2 (kWh/kg of Mg)	2.5*	<10
CO_2 emissions associated with cell internal energy consumption (kg/kg Mg)	1	<4
Electrorefining current efficiency (pct)	~100	>90
Mg recovery at the cathode (pct)	>93	>90
Mg recovery in the cathode product alloy (pct)		
H_2 evolution	96	>90
Recovered Mg weight	87~100	
CO_2 emissions* @ 2.5 kWh/kg of Mg (kg CO_2/kg Mg)	<1*	<4
Production cost ($/kg) (same for Al and Mg products)	$1.6–1.7	<$2

*Not including energy required to melt scrap.

Table III. Mg Cathode Product Elemental Composition for the 84 LiF + 16 MgF_2 Electrolyte at 1073 K (800 °C) (ICP wt pct)

	Sample		
Wt Pct	#1	#2	Comments
Mg	98.60	99.66	high selectivity for Mg
Al	0.86	0.0630	variable between Mg droplets:
Li	0.54	0.2200	different current density
Na	0.0055	0.0075	different Mg pct in Al
Mn	<0.0010	0.0011	
Fe	0.0106	0.0021	(Si + Fe) 0.02~0.04 pct << 0.3 pct target
Zn	0.0015	0.0016	(Si + Fe + Cu + Zn + Mn + Co) 0.025~0.046 pct
Si	0.0077	0.0395	no electrolytic transfer to cathode
Cu	<0.0010		prime purity product
Co	0.0035	0.0015	

The cathode product analyzed by ICP was recovered from the cathode surface during cell post-mortem.

Table IV. Al Anode Product Elemental Composition for the 84 LiF + 16 MgF_2 electrolyte at 1073 K (800 °C) (ICP wt pct)

Wt Pct	Start	End	Comment
Al	95.56	98.80	Al concentrates as Mg is moved to the cathode
Mg	3.35	0.14	20 times reduction, 95 pct Mg removed
Mn	0.547	0.543	
Fe	0.222	0.292	
Zn	0.150	0.153	no change, no undesirable electrolytic transfer to the cathode product
Si	0.062	0.055	
Cu	0.345		
Co	0.007	0.006	
Li	0.102	0.009	<<0.05 pct, 10 times reduction during electrorefining, 90 pct Li removed
Na	0.0019	0.0014	no change

(ICP wt pct).

Advantages of this electrolyte are as follows:

1. A chemically simple binary electrolyte system with a high content of Li^+ current carriers and sufficient Mg^{2+} at the target density of ~2 g/cm^3.
2. The highest ionic electrical conductivity combined with the lowest electronic conductivity allowing the potential for a very high current efficiency of Mg production by electrorefining.
3. Low electrolyte viscosity promoting circulation, Mg metal product separation and filtration.
4. No Mg^{2+} complexes resulting in the high mobility of Mg^{2+} in the electrolyte.
5. Not very hygroscopic.
6. Superheat in the right range for liquid containment in electrolyte freeze.

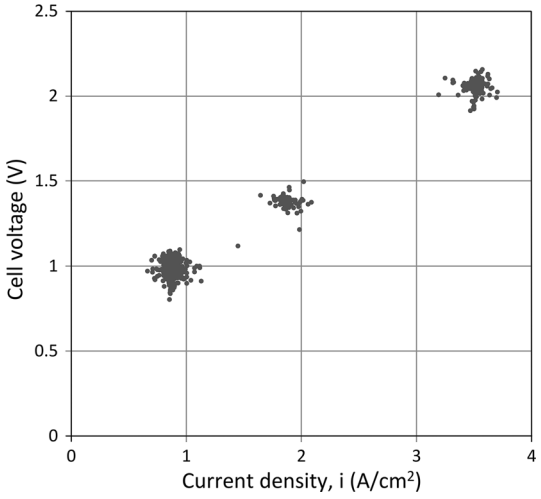

Fig. 20—Cell voltage for 84 LiF + 16 MgF_2 electrolyte at 1073 K (800 °C).

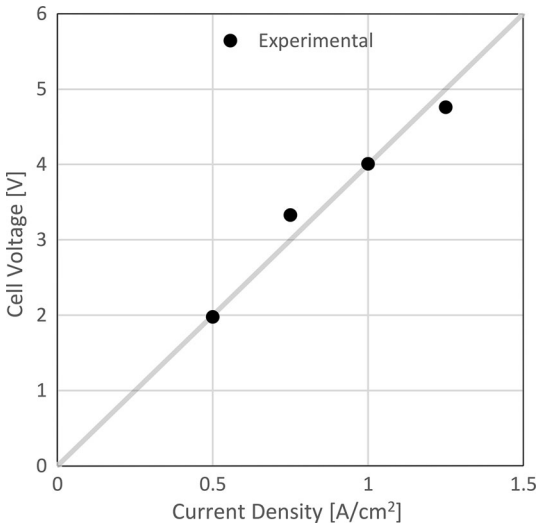

Fig. 21—Measured cell voltage in 44 NaCl + 26 $MgCl_2$ + 30 $SrCl_2$ electrolyte at ACD of ~ 8 cm and 1023 K (750 °C).

The disadvantages are as follows:

1. Experimentally, there is 0.2 wt pct Li in the Mg cathode metal. This is very close to a predicted value of 0.29 wt pct.

B. *Chloride Electrolytes*

There are three potential chloride systems: 44 NaCl + 26 ± 10 $MgCl_2$ + 30 $SrCl_2$; 32 LiCl + 36 ± 8 $MgCl_2$ + 32 $SrCl_2$; and 44 KCl + 20 ± 8 $MgCl_2$ + 36 $SrCl_2$. A NaCl-containing system was selected for experimental testing based on the extreme hygroscopicity of LiCl and lower ionic conductivity of KCl.

Advantages:

1. Low cost
2. Low viscosity

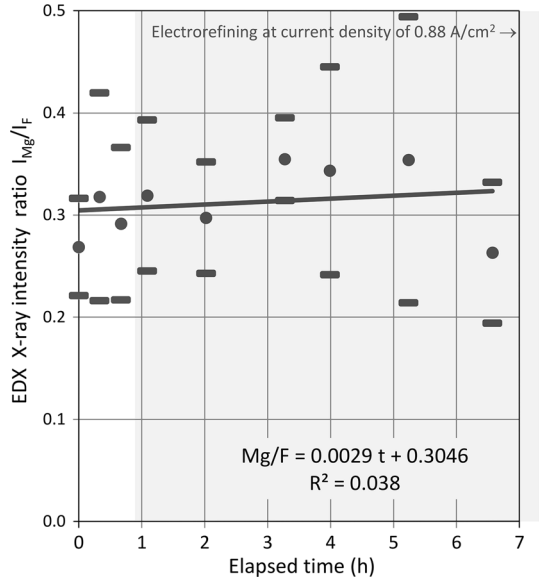

Fig. 22—84 LiF + 16 MgF_2 electrolyte chemical composition stability over time at 1073 K (800 °C) as measured by the EDX X-ray intensity ratio I_{Mg}/I_F.

Disadvantages:

1. Experimentally, 2.5 wt pct Na and 0.35 pct Sr in the Mg cathode product and ~ 0.02 wt pct Na in the Al anode product.
2. $MgCl_2 \cdot H_2O$ decomposes to MgO + HCl on drying.
3. High superheat → electrolyte freeze cannot be used for liquid containment.
4. Residual moisture in the molten chloride salt oxidizes Al or Mg metal melts preventing coalescence of the metal droplets. Fluoride addition is necessary to promote coalescence.

Based on this comparison of the fluoride and chloride systems, fluoride was selected for the RE-12 electrorefining process.

FactSage predictions were not all borne out experimentally. In some cases, the difference can be ascribed to the formation of protective passive surface films that prevent further reaction, such as alumina surface film on molten aluminum protecting it from further oxidation, or AlN surface film preventing conversion of BN to AlN and AlB_{12}. The electrolyte and metal melt density predictions were confirmed by experiments. The electrical conductivity of chloride electrolyte predicted the measured cell voltage exactly, indicating that overpotentials and other internal cell resistances were small. For the fluoride electrolyte, the measured cell voltage was actually smaller than the electrolyte resistance voltage drop predicted based on the FactSage electrical conductivity. This would imply that either the electrolyte conductivity is actually higher than predicted, or that the other geometric cell factors, such as lower-than-expected ACD, contributed to the measured low cell voltage. Higher ionic conductivity is indeed possible, since the ionic conductivity of the LiF-MgF_2 liquid was estimated from data available for

multicomponent liquids involving LiF and MgF_2 as minor components {such as NaF-AlF_3(-CaF_2)-LiF-MgF_2 (-Al_2O_3)}.

FactSage modeling allows access to validated knowledge on thermodynamic properties of compounds and solutions that, combined with the software reaction, equilibrium, and phase diagram software, allows a nonexpert user to make thermodynamically valid predictions for new, yet untested combinations of the components contained in the thermodynamic databases. FactSage does not allow the user to make predictions for components or materials that have not been entered into the database. While expert users can develop their own database for the new compounds and solutions, our objective was to use the best available knowledge to select the electrolyte for a novel electrorefining process. In that, with the help of FactSage and their team at Ecole Polytechnique, we succeeded well.

VIII. CONCLUSIONS

Phase diagram and thermodynamic modeling significantly shortened the time required for the RE-12™ process proof-of-concept by allowing to determine the preferred electrolyte composition in a single experimental cycle, and by giving reliable material composition property and reactivity prediction for the products as well as for the materials of construction.

ACKNOWLEDGMENTS

The authors gratefully acknowledge the financial and the technical assistance provided by the United States Department of Energy Advanced Research Project Agency (US DOE ARPA-e). Extensive technical, economic, and business discussions with James Klausner (Program Director), Bahman Abbasi, Thomas Bucher, and Daniel Matuszak were very helpful. Ray Peterson of Real Alloy provided aluminum scrap samples and industrial inputs regarding commercialization. The authors thank David Thweatt, Kevin Loutfy, Y. Kim, Jay DeSilva, Charles Ibrahim, and Mr. Robert Hoffman at MER Corporations well as Mark Gesing of Gesing Consultants Inc. all contributed significantly to the experimental process validation. The authors also thank the FactSage group at the Ecole Polytechnique, Arthur Pelton, Christian Robelin, and Aimen Gheribi for excellent training and support throughout the thermodynamic modeling effort including electrolyte electrical conductivity estimates.

REFERENCES

1. A.J. Gesing, S.K. Das, and R.O. Loutfy: *JOM*, 2016, vol. 68 (2), pp. 585–93.
2. A.J. Gesing, S. Das, and M. Gesing: US Patent Application US 2015/0225864 A1, 2015 (Phinix, LLC).
3. Phinix, LLC - Trade Mark: RE12TM Recycled Magnesium, 2014.
4. Advanced Research Project Agency - Energy (ARPA-e) of the US Department of Energy - Funding Opportunity No. DE-FOA-0000882, March 20, 2013.
5. FactSage - http://www.crct.polymtl.ca/fact/.
6. P. Chartrand and A.D. Pelton: *Metall. Mater. Trans. A*, 2001, vol. 32A, pp. 1417–30.
7. E. Renaud, C. Robelin, A.E. Gheribi, and P. Chartrand: *J. Chem. Thermodyn.*, 2011, vol. 43, pp. 1286–98.
8. Y. Tanga, Y. Dua, L. Zhanga, X. Yuana, and G. Kaptay: *Thermochim. Acta*, 2012, vol. 527, pp. 131–42.
9. H.C. Gaur and H.L. Jindal: *Electrochim. Acta*, 1970, vol. 15 (7), pp. 1127–34.
10. H.C. Gaur and W.K. Behl: *Electrochim. Acta*, 1963, vol. 8 (3), pp. 107–14.
11. H.C. Gaur, W.K. Behl, Electrochemistry, 1965, pp. 543-55.
12. H.C. Gaur and H.L. Jindal: *Electrochim. Acta*, 1968, vol. 13 (4), pp. 835–42.
13. J. Sangster and A.D. Pelton: *J. Phys. Chem. Ref. Data*, 1987, vol. 16 (3), pp. 509–61.
14. Y. Dessureault, J. Sangster, and A.D. Pelton: *J. Chim. Phys.*, 1990, vol. 87 (3), pp. 407–53.
15. J. Sangster and A.D. Pelton: *Phase Equilib.*, 1991, vol. 12 (5), pp. 511–37.
16. P. Chartrand and A.D. Pelton: *Can. Metall. Quart.*, 2000, vol. 39 (4), pp. 405–20.
17. P. Chartrand and A.D. Pelton: *Metall. Mater. Trans. A*, 2001, vol. 32A, pp. 1361–83.
18. P. Chartrand and A.D. Pelton: *Metall. Mater. Trans. A*, 2001, vol. 32A, pp. 1385–96.
19. P. Chartrand and A.D. Pelton: *Canad. Metall. Quart.*, 2000, vol. 40 (1), pp. 13–32.
20. P. Chartrand and A.D. Pelton: *Light Metals*, 2002, vol. 2002, pp. 245–52.
21. C. Robelin, P. Chartrand, and A.D. Pelton: *J. Chem. Thermodyn.*, 2004, vol. 36 (9), pp. 793–808.
22. C. Robelin, P. Chartrand, and A.D. Pelton: *J. Chem. Thermodyn.*, 2004, vol. 36 (9), pp. 809–28.
23. C. Robelin, P. Chartrand, and A.D. Pelton: Thermodynamic Evaluation and Optimization of the NaCl-KCl-AlCl3 System*J. Chem. Thermodyn.*, 2004, vol. 36 (8), pp. 683–99.
24. C. Robelin: Master's Thesis, Ecole Polytechnique, Montreal, 1997.
25. J. Sangster: *J. Phase Equilib.*, 2000, vol. 21 (3), pp. 241–68.
26. A.D. Pelton, S.A. Degterov, G. Eriksson, C. Robelin, and Y. Dessureault: *Metall. Mater. Trans. B*, 2000, vol. 31B, pp. 651–59.
27. A.D. Pelton and P. Chartrand: *Metall. Mater. Trans. A*, 2001, vol. 32A, pp. 1355–60.
28. A.D. Pelton, P. Chartrand, and G. Eriksson: *Metall. Mater. Trans. A*, 2001, vol. 32A, pp. 1409–16.
29. C. Robelin, P. Chartrand, and G. Eriksson: *Metall. Mater. Trans. B*, 2007, vol. 38B, pp. 869–79.
30. C. Robelin and P. Chartrand: *Metall. Mater. Trans. B*, 2007, vol. 38B, pp. 881–92.
31. E.G. Wilson: *Phys. Rev. Lett.*, 1963, vol. 10 (10), pp. 432–34.
32. P.J. Durham and D.A. Greenwood: *Philos. Mag.*, 1976, vol. 33 (3), pp. 427–40.
33. M. Shimoji and K. Ichikawa: *Phys. Lett.*, 1966, vol. 20 (5), pp. 480–81.